MICROSTRUCTURAL EVOLUTION AND SELF-ORGANIZATION OF SHEAR BANDS

M.A. Meyers[1], Q. Xue[1], Y. Xu[2], and V.F. Nesterenko[1]

[1]University of California, San Diego, La Jolla, CA 92093, USA
[2] Institute of Metals Research, CAS, China

ABSTRACT

Hat-shaped specimens deformed in a Hopkinson bar and specimens recovered from the collapse of thick-walled cylinders were used to generate strain rates of approximately $10^4 s^{-1}$ and shear strains that could be varied between 1 and 100. Shear bands were generated in Al-Li, Ti, Ti-6%Al-4%V alloy, AISI 304L SS. Transmission electron microscopy reveals, for Al-Li and AISI 304L SS, a number of features that include the observation of grains with sizes in the nanocrystalline domain. An evolutionary model, leading from the initial grain size of 15 μm to the final submicronic (sub) grain size describes the microstructural changes, by rotational dynamic recrystallization.

The shear-band initiation, propagation, as well as spatial distribution were examined under different global strains. The shear bands nucleate at the internal boundary of the cylindrical specimens and construct a periodical distribution at an early stage. The evolution of shear-band pattern during the deformation process reveals a self-organization character. The experimental shear-band spacings are compared with theoretical predictions that use the perturbation analysis and momentum diffusion. A new two-dimensional model is proposed for the initiation and propagation that treats initiation as a probabilistic process with a Weibull dependence on strain; superimposed on this, a shielding factor is introduced to deal with the disactivation of embryos.

KEYWORDS

shear bands, self organization, dynamic recrystallization, recrystallization

1 EXPERIMENTAL TECHNIQUES

Shear bands were generated by two methods:

(a) The hat-shaped specimen method, Fig. 1(a), uses a split Hopkinson bar in the compression mode to generate large shear strains in a small region (~200μm thick). This method was developed by Meyer and Manwaring (1986) and has been successfully used to generate shear localization regions in a number of metals (e.g., Andrade et al., 1994).

(b) The explosive collapse of a thick-walled cylinder under controlled and prescribed conditions. The experimental procedure consisted of subjecting thick-walled cylinders to controlled collapse by means of explosives placed on the periphery, in a cylindrical geometry with initiation at one of

the extremities. Nesterenko and Bondar (1994) and Nesterenko et al. (1998) describe the procedure in detail. Selected dimensions of copper tubes sandwiched in the sample control the collapse of thick-walled cylinder specimen. Figure 1(b) shows the process of cylinder collapse, with the shear bands marked schematically. They have spiral trajectories and initiate at the internal surface of the cylinder. The strain rate imparted is on the order of $10^4 s^{-1}$. The collapse of the cylinder generates the highest shear strains along the internal surface. The unstable deformation, which is initially homogeneous, gives rise to shear bands along the internal surface. These bands grow inward to the thick-walled cylinder. The shear band spacing, L_i , length, l_i , and the edge displacements, δ_i, were measured at different global strains.

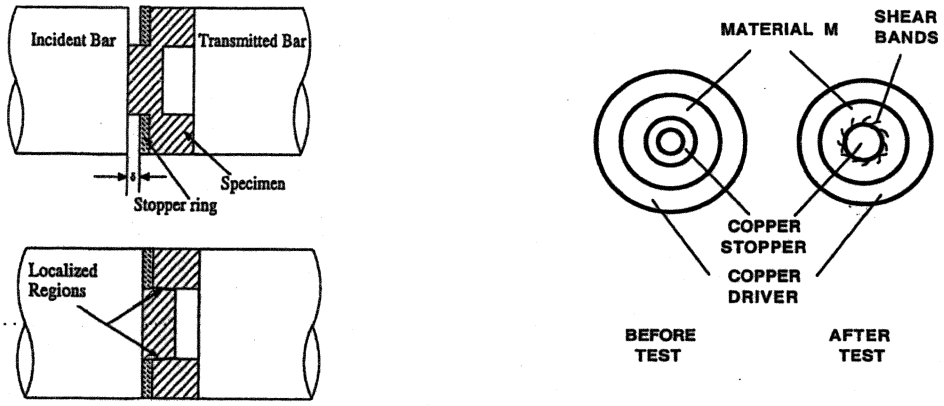

(a) (b)

Figure 1. Experimental methods used to generate shear bands; (a) Hat-shaped specimen; (b) Thick-walled cylinder specimen

2 TRANSMISSION ELECTRON MICROSCOPY

The AISI 304 stainless steel exhibited, outside of the shear band, the structure characteristic of high-strain rate deformation, which had been systematically identified earlier by Staudhammer et al. (1981). It is characterized by twins and stacking faults, propitiated by the low stacking-fault energy of 304 SS. The microstructure inside of the shear band was radically different. Two principal domains could be identified:

(a) A region composed of nanoscale grains. Figure 2(a) shows these regions for 304 SS in both bright and dark field TEM. The grains are approximately 100-200 nm in diameter. These grains have clear boundaries and are equiaxed. This structure is similar to the ones observed in titanium (Meyers and Pak, 1986), copper (Andrade et al., 1994), Al-Li (Xu et al., 2001), and brass (Li et al., 2000). For an Al-Li alloy, the features shown in Figure 2(a) are analogous to the ones for 304SS. This has been attributed to a rotational recrystallization mechanism, which was proposed and quantitatively expressed by Meyers et al. (1997, 2001). Mataya, Carr, and Krauss (1982) were the first to analyze shear bands in stainless steel and they correctly identified the mechanism for the formation of these grains. Figure 3 shows the sequence of events leading to rotational dynamic recrystallization.

(b) A glassy region separated from the nanocrystalline region by an interface. Figure 4 shows this interface, with the glassy region at the right and the crystalline one at the left. High-resolution transmission electron microscopy confirms the amorphous nature of the material. This is a surprising finding and the first observation of a crystalline to amorphous transition in a shear band. Barbee et al. (1979) were able to produce the amorphous transition in 304 SS by sputter depositing it. However, this was only possible for a carbon concentration greater than 5 at.%.

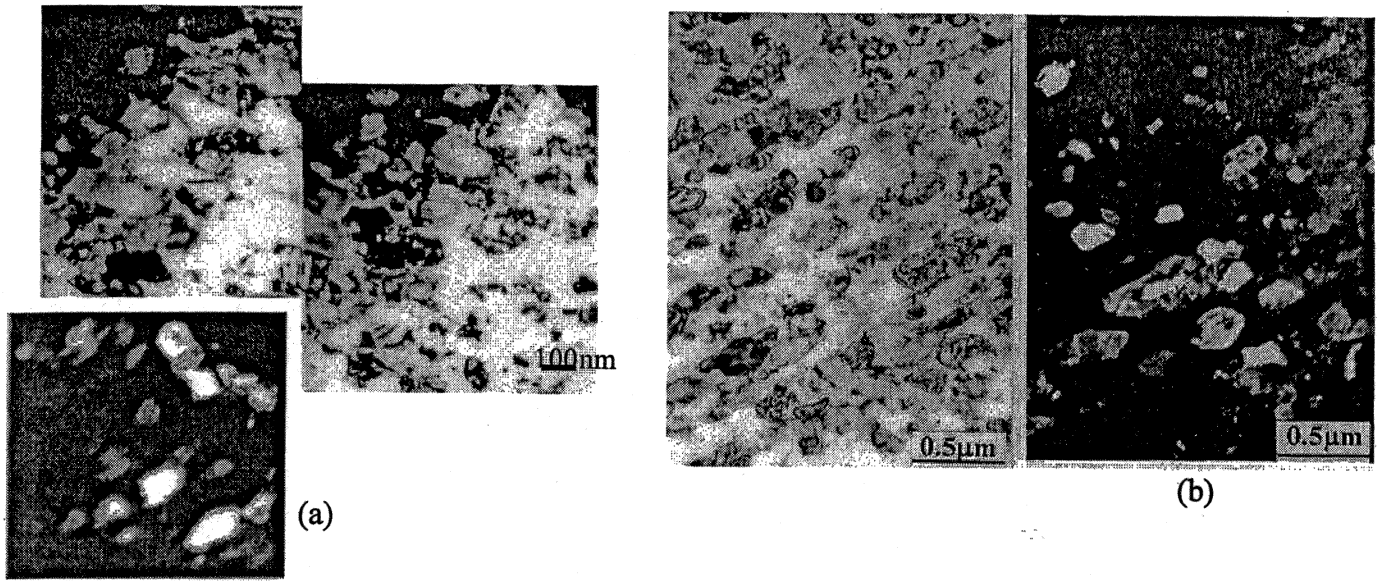

Figure 2: (a,b)Microcrystalline structure (d~100-200nm) and dark fields inside bands of (a)AISI 304 SS and (b)Al-Li alloy.

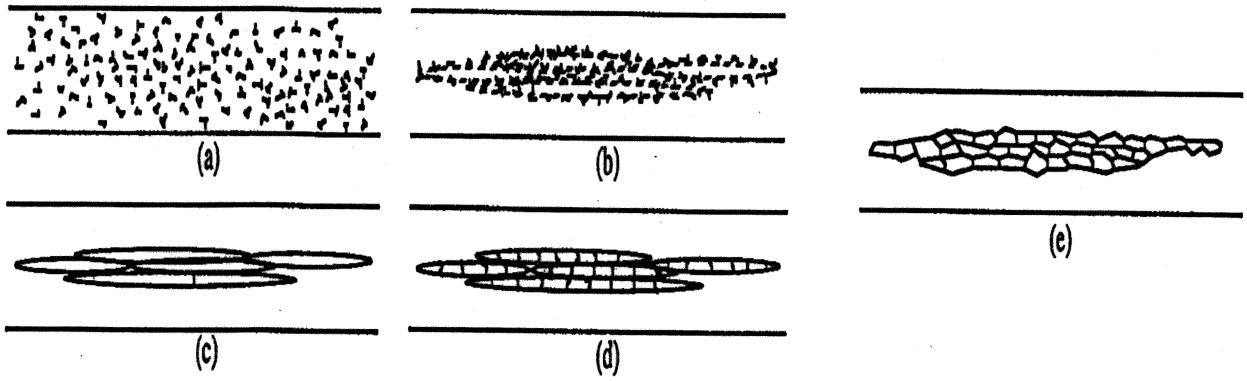

Figure 3: Schematic illustration of microstructural evolution during high-strain-rate deformation. (a) Randomly distributed dislocations; (b) Elongated dislocation cell formation; (c) Elongated subgrain formation; (d) Initial break-up of elongated subgrains; and (e) Recrystallized microstructure

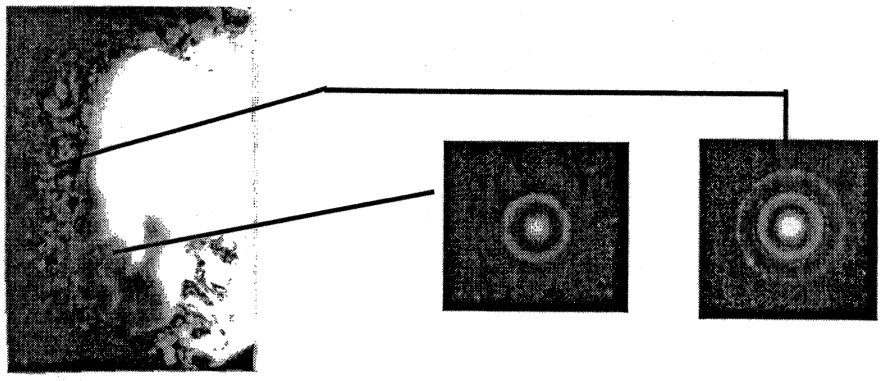

Figure 4: Interface between nanocrystalline and amorphous regions.

3 MEASURED AND PREDICTED SHEAR BAND SPACINGS

Most of the studies till this date have focused on a single band and assumed a one-dimensional configuration. Notable exceptions are the experimental contributions of Bowden (1980) in polymers and Shockey and Erlich (1981) in steels, and the analyses developed by Grady (1980), Wright and Ockendon (1996), Grady and Kipp (1987), and Molinari (1997).
Grady (1980) was the first to propose a perturbation solution to shear instability of brittle materials. Wright and Ockendon (1996) also developed a theoretical model, based on small perturbations. The predicted spacing is expressed as:

$$L_{WO} = 2\pi\left(\frac{m^3 kC}{\dot{\gamma}_0^3 a^2 \tau_0}\right)^{1/4} \tag{2}$$

Where a is the thermal softening coefficient; k is the thermal conductivity; C is the heat capacity; τ_0 is the shear flow stress; $\dot{\gamma}_0$ is the strain rate; and m is the strain rate sensitivity. Grady and Kipp (1986) extended Mott's (1947) analysis for dynamic fracture to deformation localization. Momentum diffusion was considered as the dominant mechanism of shear bands. The spacing is:

$$L_{GK} = 2\left[\frac{9kC}{\dot{\gamma}_0^3 a^2 \tau_0}\right]^{1/4} \tag{3}$$

Molinari (1997) modified the WO model by introducing strain-hardening effect:

$$L_{M'} = 2\pi\left[1-\frac{3}{4}\frac{\rho c}{\beta\tau_0^2}\frac{n(1-aT)}{\beta a\gamma}\right]^{-1}\cdot\left[\frac{kCm^3(1-aT_0)^2}{(1+m)\dot{\gamma}_0^3 a^2\tau_0}\right]^{1/4} \tag{4}$$

Where n is the strain-hardening index.
The measured spectra of shear bands in 304SS, CP titanium and Ti-6Al-4V alloy obtained by the thick-walled cylinder method are shown in Figure 5 at two global effective strains: 0.55 and 0.92 (for 304SS and CP Ti, Figs 5(a)-(f)); 0.13 and 0.26 (for Ti-6Al-4V, Fig. 5(g,h)). The numbers of shear bands at both the early and later stages are similar in SS 304 and Ti. There is no significant effect of grain size on shear band patterning for 304SS from Figs. 5(a)-(d).
Table 1 shows the comparison of experimental and predicted results. The grain size has only a minor effect on the spacing for 304SS, in the range investigated. The predicted results from Grady-Kipp model are roughly 20 times larger than measured values for Ti and 304SS, and twice for Ti-6Al-4V. On the other hand, the WO and M models provide reasonable estimates for Ti and 304SS but not for Ti-6Al-4V. The failure of these theoretical predictions for Ti-6Al-4V alloy suggests that some mechanisms of shear band development have not been included into the above theories. One very important factor that is not incorporated into these theories is the two-dimensional nature of interactions among growing bands, which increases with their size. This was recognized by Nemat Nasser et al. (1976) for parallel propagating cracks. A conceptually similar analysis is presented in the next section.

4 TWO-DIMENSIONAL MODEL FOR SHEAR BAND SPACING

The failure of the one-dimensional models to explain the evolution of shear–band spacing led to proposed model below. Initiation of shear bands is assumed to require a critical strain. Heterogeneous microstructural or surface effects (boundary geometry, defects, and orientation of grains, etc.) determine the range of strains in which the nucleation takes place. A heterogeneous

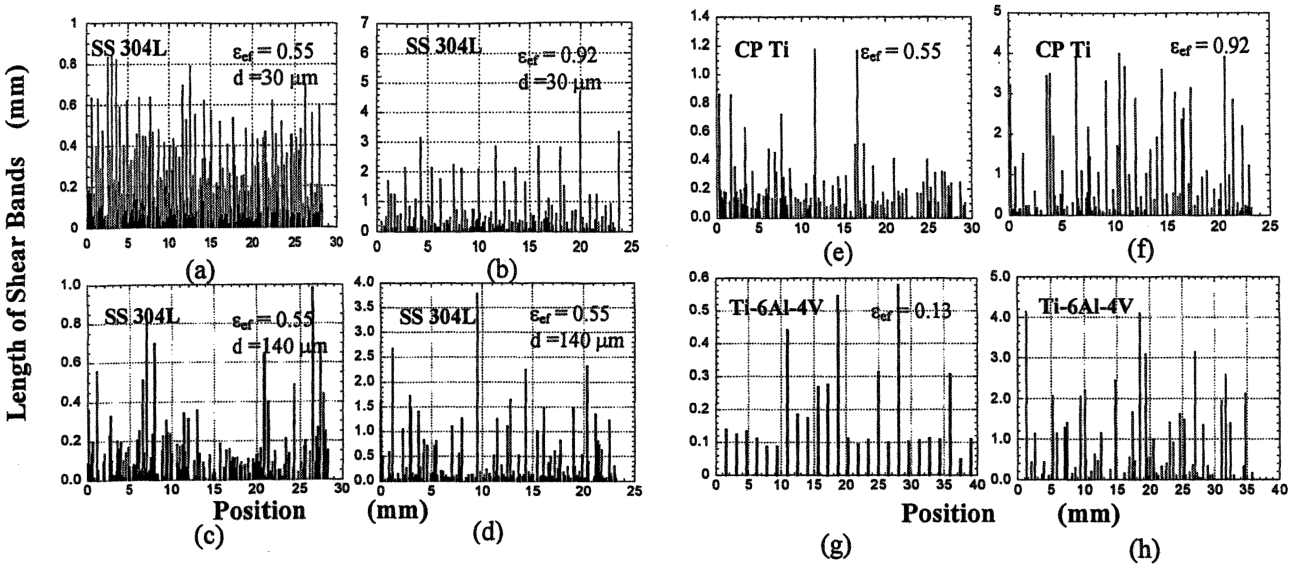

Figure 5: Configuration of shear-band lengths and spacings at different imposed strains for (a, b) AISI 304 SS, =30 μm ; (c, d) AISI 304 SS, d=140 μm; (e, f) CP titanium; (g, h) Ti-6Al-4V alloy

TABLE 1
PREDICTIONS AND EXPERIMENTAL SPACINGS FOR 304SS TI, AND TI-6%AL-4%V

Spacing(mm)	Exp. Data Initial level	L_{WO}(mm)	L_{GK}(mm)	L_{MO} (mm) (Without strain hardening)	L_{MO} (mm) (with strain hardening)
SS 304L	0.12	0.33	2.40	0.29	--
CP Titanium	0.18	0.29	2.13	0.24	0.64
Ti-6Al-4V	0.53	0.1	1.15	0.09	0.10

nucleation process, which is characterized as the selective activation of sites, will be assumed. The probability of nucleation is given by P (V_0,S_0), in a reference volume, V_0, or surface, S_0, depending on whether initiation occurs in the bulk or on the surface. It can be described by a modified Weibull distribution, using strain as the independent variable:

$$P(V_0, S_0) = 1 - \exp\left[-\left(\frac{\varepsilon - \varepsilon_i}{\varepsilon_0 - \varepsilon_i}\right)^q\right] \tag{5}$$

where ε_i am the critical strain below which no initiation takes place; ε_0 is the average nucleation strain (material constant); ε is the variable; and q is a Weibull modulus. For different materials the nucleation curve can have different shapes and positions, adjusted by setting q, ε_i, and ε_0. For Ti and Ti-6Al-4V, the mean nucleation strains are selected as 0.4 and 0.12, respectively, to best fit the experimental results; q was given values of 2, 3, 6, and 9, providing different distributions. Figures 6 (a) and (b) show the predicted distributions of initiation strains for Ti and Ti-6Al-4V, respectively.

Due to thermal softening inside bands, each growing band generates a shielded region around itself. Thus, the bands that actually grow can be a fraction of the total possible initiation sites. Three factors govern the evolution of self-organization: (a) the strain rate, $\dot{\varepsilon}$; (b) the velocity of growth of shear band, V; (c) the initial spacing, l. Different scenarios emerge, depending on the growth velocity V. The activation of embryos at three times, t_1, t_2, and t_3, is shown in Figure 7.

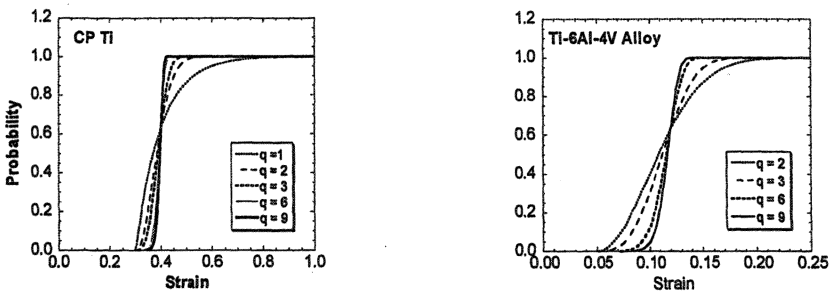

(a) (b)

Figure 6. Probability of nucleation as a function of strain for (a) CP titanium; (b) Ti-6Al-4V alloy.

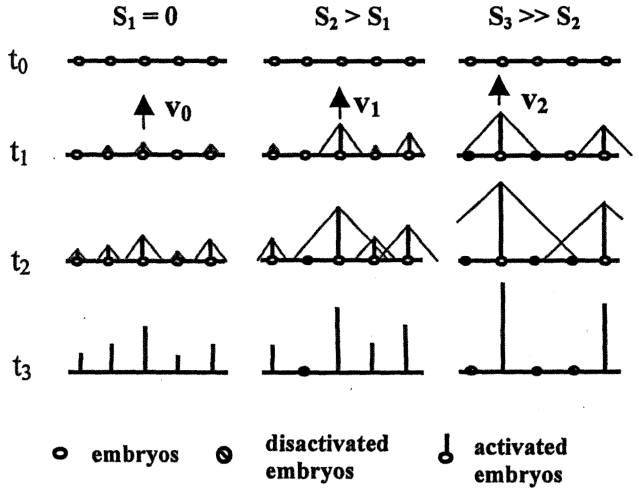

Figure 7: Two-dimensional representation of concurrent nucleation and shielding.

When V is low, the embryos are all activated before shielding can occur, and the natural spacing l_0 establishes itself. As V increases, shielding becomes more and more important, and the number of disactivated embryos increases. The shielded volume is dependent on the velocity of propagation of stress unloading and is given by k_1V, where $k_1<1$. The width of the unloaded region is $2k_1$ times the length of the shear band. The shielding effect can be expressed by S:

$$S = 1 - \frac{\dot{\varepsilon} L}{k_0 k_1 V} \tag{6}$$

k_0 defines the range of strains over which nucleation occurs. It can be set as $k_0 = 2(\varepsilon_0 - \varepsilon_i)$. It correctly predicts an increase in shielding S with increasing V, decreasing $\dot{\varepsilon}$, and decreasing L. For an extremely large velocity of propagation of shear band, the critical time is very small and the shielding factor is close to one, which means almost complete shielding. The probability of nucleation under shear band shielding, P (L), is obtained by multiplying Eqn. 5 by (1-S):

$$P(L) = \left(\frac{\dot{\varepsilon} L}{2(\varepsilon_0 - \varepsilon_i)V}\right)\left\{1 - \exp\left[-\left(\frac{\varepsilon - \varepsilon_i}{\varepsilon_0 - \varepsilon_i}\right)^q\right]\right\} \quad if \quad t_{cr} < \bar{t} \tag{7a}$$

$$P(L) = \left\{1 - \exp\left[-\left(\frac{\varepsilon - \varepsilon_i}{\varepsilon_0 - \varepsilon_i}\right)^q\right]\right\} \quad if \quad t_{cr} \geq \bar{t} \tag{7b}$$

When S = 0 no shielding effect exists and all nuclei grow. If, in other extreme case, S = 1, no nucleation can happen. Figure 8(a) shows predicted evolutions of nucleation probabilities as a function of increasing strain, for different values of the shielding factor, S: 0, 0.2, 0.4, 0.6. This simple model shows how the initial distribution of activated embryos can be affected by different parameters. Xue et al. (2001) present a more complete version of this analysis. It explains, qualitatively, the smaller spacing of shear bands in Ti, as compared to Ti-6Al-4V. The shear-band spacing, corrected for shielding, is represented by:

$$L_S = \frac{L_{WO}}{P(L)\big|_{t>\bar{t}}} = \frac{L_{WO}}{(1-S)}. \tag{8}$$

L_{WO} is the Wright-Ockendon spacing. This spacing is plotted as a function of plastic strain, at a fixed value of S, in Figure 8(b). It is clear that the shear-band spacing decreases with strain until a final, steady state value is reached (Fig.8 (b)). Using the calculated shielding factors S of 0.14 for Ti and 0. 89 for Ti-6Al-4V, the corresponding values for L_S are 0.34 and 0.9 mm, respectively. These values are in agreement with the experimental results (0.18 and 0.53 mm, respectively)

During growth, an analogous selection process takes place, leading to a discontinuous increase in the spacing of the shear bands as their length increases, as described by Xue et al (2000, 2001). At a certain length l_i, the spacing is L_i; the growth becomes unstable at a critical length $l_{cr,i}$, and alternate SB's grow with a new spacing L_{i+1}; the other shear bands stop growing. The mathematical representation of the step function is shown as:

$$L = L_0 + \sum_{j=1}^{n} k_j' \cdot H(l - l_{cr,j}) \tag{9}$$

where $H(l-l_{cr,j})$ is a Heaviside function. The parameters k_j' can be expressed as:

$$k_j' = f(V, L_0, \varepsilon_i, \varepsilon_p) \tag{10}$$

Where V is the shear band propagation velocity, L_0 is the initial spacing, ε_i is the critical strain for initiation and ε_p is the critical strain for propagation.

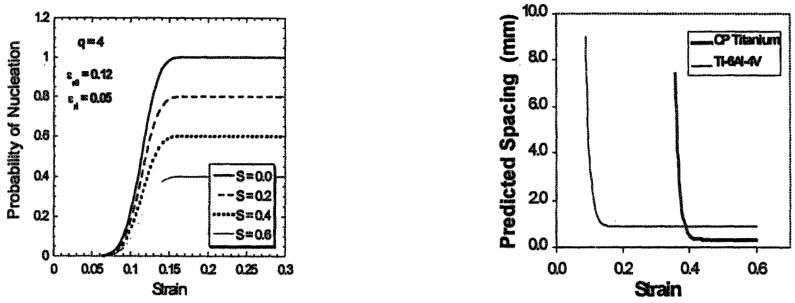

(a) (b)

Figure 8: Probability of nucleation incorporating shielding factor; (a) schematic; (b) calculated shear-band spacing for titanium and Ti-6Al-4V alloy.

5 CONCLUSIONS

The microstructural evolution inside of adiabatic shear bands in AISI 304 SS and Al- Li was observed by transmission electron microscopy and it is suggested that rotational dynamic recrystallization is responsible for the generation of the recrystallized structure with grains in the 100-300 nm domain. An amorphous region was also found in AISI 304 SS. The evolution of

multiple adiabatic shear bands was investigated in stainless steel, titanium, and Ti-6%Al-4%V alloy through the radial collapse cylinder technique under high-strain-rate deformation ($\sim 10^4$ s^{-1}). The shear-band spacing is compared with current theoretical predictions. These one-dimensional models can not provide accurate estimation of shear band spacing in Ti6%Al4%V alloy. The two-dimensional character of self-organization has to be considered. A novel analytical description, in which a distribution of embryos (potential initiation sites) is activated as a function of strain (greater than a threshold) according to a Weibull-type distribution, is proposed. The model incorporates embryo disactivation by stress shielding as well as selective growth of shear bands. The imposed strain rate, embryo distribution, and rates of initiation and propagation determine the evolution of shear band configurations.

ACNOWLEDGMENTS: Work supported by U.S. Army Research Office MURI Program No. DAAH004-96-1-0376 and by the Natural Science Foundation of China Grant No. 50071064.

6 REFERENCES

Andrade , U. R., Meyers, M. A., Vecchio, K. S., and Chokshi, A. H. (1994)., *Acta Met.*, **42**,3183-3195

Barbee, T. J. Jr., Jacobson, B. E., and Keith, D. L. (1979), *Thin Solid Films*, **63**,143-150.

Bowden, P. B. (1970), *Phil. Mag.*, **22,** 455-462.

Grady, D. E. (1980), *J. Geophys. Res.*, **85,** 913-924.

Grady, D.E., and Kipp, M.E. (1987), *J. Mech. Phys. Solids,* **35**, 95-118.

Li, Q., Xu,Y. B., Lai, Z. H., Shen, L. T., and Bai, Y. L. (2000), *Mat. Sci. Eng.*,**A276**,127.

Mataya, M. C., Carr, M. J., and Krauss, G. (1982), *Met. Trans. 133A*,1263-1274

Meyer, L. W., and Manwaring, S. (1986), in *Metallurgical Applications of Shock-Wave and High-Strain-Rate Phenomena*, M. Dekker, ,pp. 657-674.

Meyers, M. A., and Pak, H.-r. (1986), *Acta Met.*, **34**, 2493.

Meyers, M. A., LaSalvia, J. C., Nesterenko, V.F., Chen, Y. J., Kad, B. K.(1997), *Proc. 3rd Intl. Conf. Recrystallization and Related Phenomena,* (REX'96). McNelley, Ed.,p.279.

Meyers, M. A., Xue, Q., Nesterennko, V. F., LaSalvia, J. C. (2001), *Mat. Sci. Eng.,* in press.

Molinari, A. (1997), *J. Mech. Phys. Sol.* **45**, 1551-75.

Mott, N. F. (1947), *Proc. Roy. Soc.*,**189,** 300

Nemat-Nasser, S., and Keer L.M. and Parihar, K.S. (1978)., *Int. J. Solids Structures*, **14**, 409-430.

Nesterenko, V. F., and Bondar, M. P. (1994), *DYMAT J.*,**1**,243-251.

Nesterenko, V.F., Meyers, M.A., and Wright, T.W. (1998), *Acta Mat.*, **46**, 327-340

Nesterenko,V. F., Xue, Q., and Meyers, M. A. (2000), *J. Phys.*IV, **10,** 9-269-9-274.

Shockey D.A. and Erlich D.C. (1981), In *Shock Waves and High-Strain-Rate Phenomena in Metals* (eds. Meyers, M.A. and Murr, L. E.), Plenum Press, New York, pp. 249-261.

Staudhammer, K. P., Frantz, C. E., Hecker, S., S., and Murr, L. E.(1981*)*, in *Shock Waves and High-Strain –Rate Phenomena in Metals,* M. Dekker, pp.91-112.

Stout, M.G., Follansbee, P.S. (1986), *Trans. ASME., J of Eng Mat. & Tech*, **108**, 344-53.

Wright, T.W., and Ockendon, H. (1996)., *Int. Journal of Plasticity*, **12**, 927-34.

Xu, Y. B., Zhong, W. L., Chen, Y. J., Shen, L. T., Liu, Q., Bai, Y. L. and Meyers, M. A. (2001), *Mat. Sci, Eng.*,**A299**,287-295.

Xue Q., Nesterenko, V. F., and Meyers, M. A.(2000), in *Shock Compression of Condensed Matter-1999* (eds. M.D. Furnish et al.),AIP, NY,pp. 431-434.

Xue, Q., Meyers, M. A., and Nesterenko, V. F. (2001), *Acta Mat.,* submitted.

Xue, Q., Nesterenko, V. F, and Meyers, M.A. (2000), in *Shock Compression of Condensed Matter-1999* (eds. M.D. Furnish et al.), AIP, New York, pp. 431- 434.